As per UGC guidelines an electronic bar code is provided to secure your paper

International Journal for Modern Trends in Science and Technology
Volume 12, Issue 08, pages 37-50.
ISSN: 2455-3778 online
Available online at: http://www.ijmtst.com/vol12issue06.html
DOI: https://doi.org/10.5281/zenodo.22120027

Design and Control of a Grid-Connected Hybrid PV–Fuel Cell DC Microgrid with Intelligent Energy Management and Hybrid Energy Storage

Madhur. Suresh | K Suresh | M. Harish

Department of Electrical & Electronics Engineering, Sri Venkatesa Perumal College of Engineering and Technology, Puttur, Andhra Pradesh, India.

To Cite this Article
Madhur. Suresh, K Suresh & M. Harish (2026). Design and Control of a Grid-Connected Hybrid PV–Fuel Cell DC Microgrid with Intelligent Energy Management and Hybrid Energy Storage. International Journal for Modern Trends in Science and Technology, 12(08), 37-50. https://doi.org/10.5281/zenodo.22120027

Article Info
Received: 29 June 2026; Revised: 09 July 2026; Accepted: 12 July 2026.

KEYWORDS

DC microgrid, photovoltaic system, fuel cell, battery energy storage system, supercapacitor, intelligent energy management, voltage source converter, DC bus voltage regulation, power quality, renewable energy integration.

ABSTRACT

This paper proposes intelligent hybrid DC microgrid architecture for improving power management, DC bus voltage regulation, and power quality in grid-connected renewable energy systems. The proposed system integrates a solar photovoltaic (PV) array, fuel cell (FC), battery energy storage system (BESS), and supercapacitor (SC) through dedicated DC–DC boost and bidirectional buck–boost converters connected to a common 600 V DC bus. A three-phase voltage source converter (VSC) interfaced with an LCL filter enables bidirectional power exchange between the DC microgrid and the utility grid while supplying both linear and nonlinear loads. An intelligent energy management controller (IEMC) is developed to coordinate power sharing among the renewable sources and energy storage devices based on source availability, load demand, DC bus voltage, and battery state of charge. The proposed control strategy prioritizes photovoltaic generation under normal operating conditions, utilizes the fuel cell during renewable power deficiency, and employs the battery and supercapacitor to compensate for long-term and transient power imbalances, respectively. Consequently, excessive charging and discharging of the battery are significantly reduced, enhancing storage lifetime and overall system reliability. Furthermore, the VSC performs active power injection, reactive power compensation, harmonic mitigation, and grid synchronization to improve power quality at the point of common coupling. The proposed architecture maintains a stable DC bus voltage under varying solar irradiance, dynamic load conditions, and grid disturbances while ensuring efficient utilization of renewable resources. Simulation and experimental investigations under different operating modes demonstrate that the proposed system achieves superior dynamic response, improved power sharing capability, reduced DC bus voltage fluctuations, lower harmonic distortion, and enhanced operational stability compared with

I. Introduction

The increasing global demand for electrical energy, rapid depletion of fossil fuel resources, and growing environmental concerns have accelerated the deployment of renewable energy resources (RESs) in modern power systems. Solar photovoltaic (PV) and fuel cell (FC) technologies have emerged as promising clean energy sources because of their environmental sustainability, high efficiency, and low carbon emissions [1]–[3]. The integration of distributed renewable generation has significantly contributed to the development of microgrids, which provide an efficient platform for supplying local loads while improving system reliability, energy efficiency, and operational flexibility [4], [5]. Among various microgrid architectures, DC microgrids have attracted considerable attention because renewable energy sources, battery storage systems, electric vehicles, and many modern electronic loads naturally operate on DC power. Compared with conventional AC microgrids, DC microgrids eliminate unnecessary power conversion stages, reduce energy losses, simplify control implementation, and improve overall system efficiency [6], [7]. Among renewable energy technologies, photovoltaic systems have become one of the most widely adopted solutions due to their modularity, low maintenance requirements, and continuous reduction in installation costs [8], [9]. However, photovoltaic power generation is highly dependent on solar irradiance and ambient temperature, resulting in intermittent and unpredictable output power. These fluctuations introduce power imbalance, DC bus voltage variations, and operational instability within the microgrid, particularly during rapidly changing weather conditions or sudden load variations [10], [11]. Consequently, maintaining continuous and reliable power supply remains one of the major challenges in renewable energy-based DC microgrids. To overcome the limitations associated with intermittent solar generation, fuel cells have been increasingly integrated with photovoltaic systems to establish hybrid renewable energy systems [12], [13]. Fuel cells provide stable and controllable electrical power independent of weather conditions, thereby complementing photovoltaic generation during periods of insufficient solar energy. The coordinated operation of photovoltaic arrays and fuel cells improves renewable energy utilization, enhances supply reliability, and reduces dependence on the utility grid [14]. Energy storage systems (ESSs) play a vital role in balancing the mismatch between renewable energy generation and load demand while maintaining stable microgrid operation [15]. Battery energy storage systems (BESSs) are widely employed because of their high energy density and capability to provide long-duration energy support. However, batteries experience accelerated degradation when subjected to frequent charging and discharging cycles caused by renewable intermittency and dynamic load variations [16]. Excessive battery cycling increases thermal stress, reduces storage capacity, shortens battery lifetime, and increases replacement costs. Therefore, improving battery utilization while reducing unnecessary charging and discharging has become an important research objective [17]. Hybrid energy storage systems combining batteries and supercapacitors have recently received significant attention because they combine the high energy density of batteries with the high power density and fast dynamic response of supercapacitors [18]. In such configurations, the battery supplies long-term energy requirements, whereas the supercapacitor rapidly compensates transient power fluctuations and sudden load disturbances. This coordinated operation effectively reduces battery current stress, enhances system dynamic performance, and extends battery service life [19], [20]. The integration of multiple renewable sources and hybrid energy storage devices requires an efficient energy management strategy capable of coordinating power sharing under varying operating conditions. Conventional energy management techniques are generally based on fixed operating rules, threshold-based switching, or predefined control logic [21]. Although these methods are relatively simple to implement, they often exhibit poor adaptability under fluctuating renewable generation and dynamic load conditions. As a result, they may lead to inefficient renewable energy utilization, poor DC bus voltage regulation, increased battery degradation, and reduced overall system performance. Consequently, intelligent energy management approaches have attracted considerable research interest because of their capability to provide adaptive decision-making, optimal power sharing, and improved operational flexibility [22], [23].

In addition to energy management, maintaining high power quality in grid-connected DC microgrids remains an important technical challenge. The increasing penetration of renewable energy converters and nonlinear loads introduces harmonic distortion, voltage fluctuations, and reactive power demand, which adversely affect both utility networks and sensitive electrical equipment [24]. Voltage Source Converters (VSCs) equipped with advanced control techniques have become the preferred interface between DC microgrids and AC utility systems because they enable bidirectional power flow, regulate the DC bus voltage, inject active power, compensate reactive power, and suppress current harmonics. The incorporation of LCL filters further improves converter performance by attenuating switching harmonics and ensuring compliance with power quality standards [25], [26]. Motivated by these challenges, this paper proposes an intelligent energy management controller (IEMC) for a grid-connected hybrid DC microgrid integrating a solar photovoltaic array, fuel cell, battery energy storage system, and supercapacitor. The photovoltaic array and fuel cell are connected to a common 600 V DC bus through dedicated DC–DC boost converters, while the battery and supercapacitor are interfaced through bidirectional buck–boost converters for efficient energy exchange. A three-phase Voltage Source Converter equipped with an LCL filter enables seamless bidirectional power transfer between the DC microgrid and the utility grid while supplying both linear and nonlinear loads. The proposed IEMC continuously monitors renewable power generation, load demand, DC bus voltage, and battery state of charge to coordinate optimal power sharing among all available energy resources [27]. The battery is utilized for long-term energy balancing, whereas the supercapacitor compensates for transient power variations, thereby minimizing battery stress and extending its operational lifetime. Furthermore, the proposed control strategy improves renewable energy utilization, maintains stable DC bus voltage, enhances power quality through harmonic mitigation and reactive power compensation, and ensures reliable microgrid operation under varying operating conditions. Simulation results demonstrate that the proposed hybrid DC microgrid achieves improved power sharing, enhanced voltage regulation, reduced harmonic distortion, and superior dynamic performance compared with conventional DC microgrid architectures [28].

The main contributions of this paper are summarized as follows:

- Development of a grid-connected hybrid PV–fuel cell DC microgrid incorporating battery and supercapacitor hybrid energy storage.
- Design of an Intelligent Energy Management Controller (IEMC) for adaptive power sharing among renewable sources, energy storage devices, and the utility grid.
- Implementation of a hybrid battery–supercapacitor energy management strategy to reduce battery degradation and improve transient power compensation.
- Integration of a VSC with LCL filter for bidirectional power exchange, DC bus voltage regulation, harmonic mitigation, reactive power compensation, and grid synchronization.
- Validation through simulation under multiple operating conditions, demonstrating enhanced power quality, efficient renewable energy utilization, improved DC bus voltage regulation, and superior overall system stability.

II. System Configuration

The proposed system is a grid-connected hybrid DC microgrid integrating a solar photovoltaic (PV) array, fuel cell (FC), battery energy storage system (BESS), and supercapacitor (SC), as shown in Fig. 1. The PV array and fuel cell are connected to a common 600 V DC bus through dedicated DC–DC boost converters, while the battery and supercapacitor are interfaced using bidirectional buck–boost converters to enable charging and discharging operations. A three-phase Voltage Source Converter (VSC) with an LCL filter facilitates bidirectional power exchange between the DC microgrid and the utility grid while supplying both linear and nonlinear loads. An Intelligent Energy Management Controller (IEMC) coordinates the operation of all energy sources and storage devices based on renewable power availability, load demand, DC bus voltage, and battery state of charge. The PV array acts as the primary power source, whereas the fuel cell provides supplementary power during low solar generation. The battery supplies long-term energy support, while the supercapacitor compensates for transient power fluctuations, thereby reducing battery stress and improving dynamic response. The VSC maintains DC bus voltage, enables active and reactive power control, mitigates harmonics, and ensures grid synchronization, resulting in enhanced power quality and reliable microgrid operation.

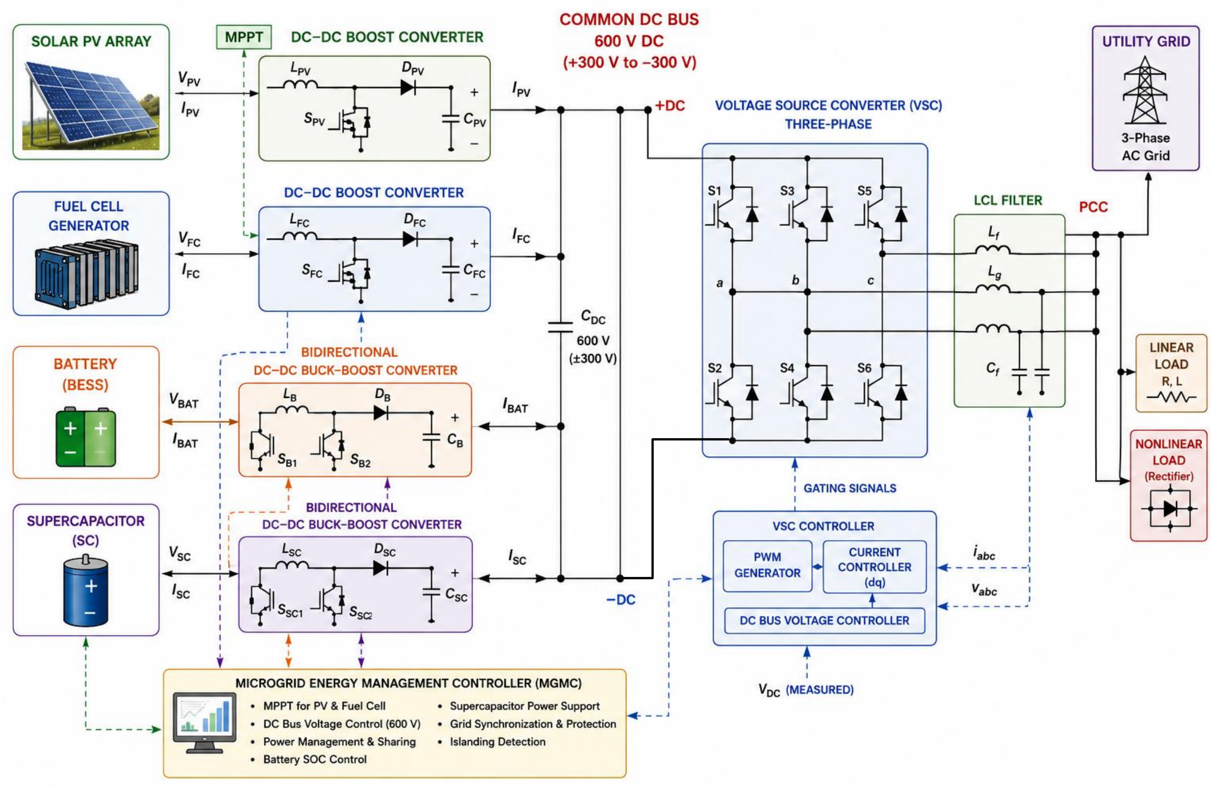

Fig.1 Proposed Method configuration

III. Solar Photovoltaic System Modeling and MPPT Control

A. System Configuration

The photovoltaic (PV) system serves as the primary renewable energy source in the proposed hybrid DC microgrid. As illustrated in Fig. 2, the PV array is connected to the common 600 V DC bus through a DC–DC boost converter. The converter consists of an input inductor L, power switch SPV, diode D, and output capacitor C. A Perturb and Observe (P&O)-based Maximum Power Point Tracking (MPPT) algorithm continuously determines the optimum operating voltage of the PV array. The reference voltage generated by the MPPT algorithm is compared with the measured PV voltage, and the resulting error is processed through a PI controller. The PI controller produces the duty cycle for the PWM generator, which controls the switching operation of the boost converter. Consequently, the PV array continuously operates at its maximum power point while maintaining the required DC bus voltage.

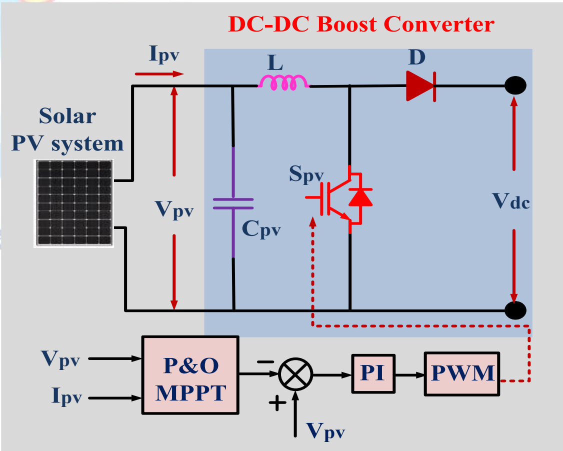

Fig.2 PV system with P&O MPPT-controlled boost converter.

B. Single-Diode Photovoltaic Modeling

The photovoltaic array is represented using the single-diode equivalent circuit, which consists of a photocurrent source, a diode, a series resistance Rs, and a shunt resistance Rsh. The output current of the PV module is expressed as

$$I_{PV} = I_{ph} - I_D - I_{sh} \quad (1)$$

where

- I_{PV} = PV output current (A)
- I_{ph} = photocurrent (A)
- I_D = diode current (A)
- I_{sh} = shunt leakage current (A)

The diode current is

$$I_D = I_o\left[exp\left(\frac{V_{PV}+I_{PV}R_S}{nV_T}\right)-1\right] \quad (2)$$

Where

$$V_T = \frac{kT}{q}$$

The shunt current is

$$I_{sh} = \frac{V_{PV}+I_{pV}R_S}{R_{sh}} \quad (3)$$

Therefore, the complete PV current equation becomes

$$I_{PV} = I_{Ph} - I_0\left[exp\left(\frac{V_{PV}+I_{PV}R_S}{nV_T}\right)-1\right] - \frac{V_{PV}+I_{PV}R_S}{R_{sh}} \quad (4)$$

The output power of the PV array is

$$V_{dc} = \frac{V_{PV}}{1-D} \quad (5)$$

Where

- D = duty ratio.

The required duty cycle is

$$D = 1 - \frac{V_{PV}}{V_{dc}} \quad (6)$$

The boost inductor is selected as

$$L = \frac{V_{PV}D}{f_S \Delta I_L} \quad (7)$$

where

- f_s = switching frequency
- ΔI_L = inductor current ripple.

The output capacitor is

$$C = \frac{I_o D}{f_S \Delta V_0} \quad (8)$$

Where

- I_o = output current
- ΔV_0 = output voltage ripple.

C. Perturb and Observe (P&O) MPPT Algorithm

To maximize the energy extracted from the PV array, a Perturb and Observe (P&O) MPPT algorithm is employed as shown in Fig.3. The controller periodically measures the PV voltage and current and computes the output power

$$P(k) = V(k)I(k) \quad (9)$$

The variations in power and voltage are calculated as

$$\Delta P = P(k) - P(k-1) \quad (9)$$

$$\Delta V = V(k) - V(k-1) \quad (10)$$

The operating voltage is updated according to the following decision rules:

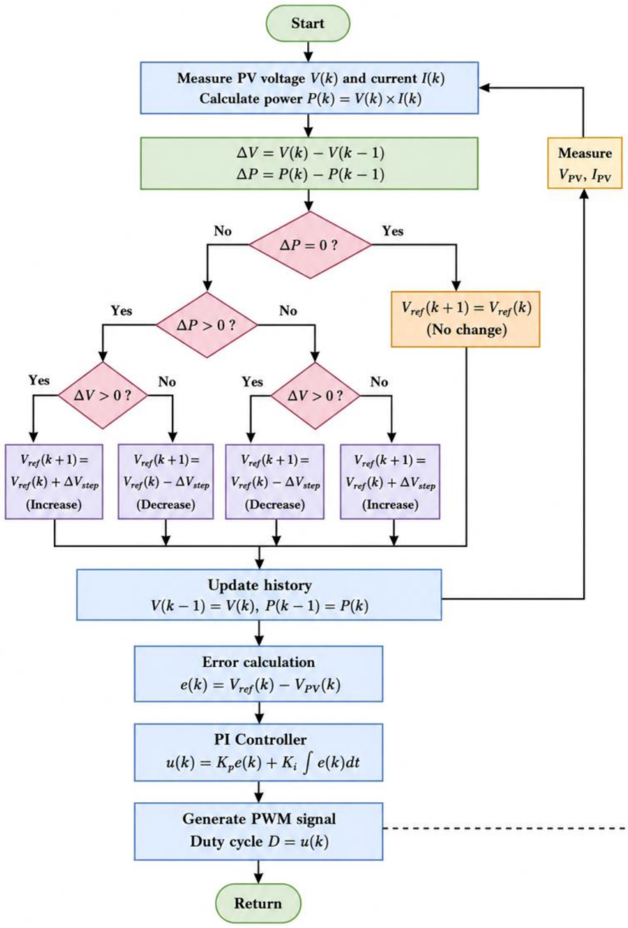

Fig. 3. Flowchart of the P&O MPPT algorithm.

- If

$\Delta P > 0$, $\Delta V > 0$ (11)

increase the reference voltage.

- If

$\Delta P > 0$, $\Delta V < 0$ (12)

decrease the reference voltage.

- If

$\Delta P < 0$, $\Delta V > 0$ (13)

decrease the reference voltage.

- If

$\Delta P < 0 , \Delta V < 0$ (14)

increase the reference voltage.

The updated reference voltage is expressed as

$$V_{ref}(k-1) = V_{ref}(k) \pm \Delta V \quad (15)$$

The voltage error is

$$e(k) = V_{ref} - V_{pv} \quad (16)$$

The PI controller generates the control signal

$$u(k) = K_p e(k) + K_i \int e(k)\, dt \quad (17)$$

The PWM duty ratio is then obtained as

$$D = \frac{u(k)}{V_C} \quad (18)$$

Where V_C is the carrier signal amplitude.

By continuously updating the duty ratio, the P&O algorithm forces the PV array to operate at the maximum power point despite variations in solar irradiance and temperature. The regulated output of the boost converter maintains a stable DC bus voltage while maximizing renewable energy utilization.

IV. Fuel Cell Modeling and Boost Converter Design

A. Fuel Cell System Configuration

The fuel cell (FC) acts as the secondary renewable energy source in the proposed hybrid DC microgrid. As shown in Fig. 4, the fuel cell is interfaced to the common 600 V DC bus through a DC–DC boost converter comprising an inductor L, power switch SFC, diode D, and output capacitor C. Since the fuel cell delivers a low and variable DC voltage, the boost converter increases the output voltage to the required DC bus level. A PI controller regulates the fuel cell current by comparing the reference current IFC∗ with the measured current IFC. The controller generates the PWM duty cycle for the boost converter, thereby maintaining stable fuel cell operation and regulating power injection into the DC microgrid.

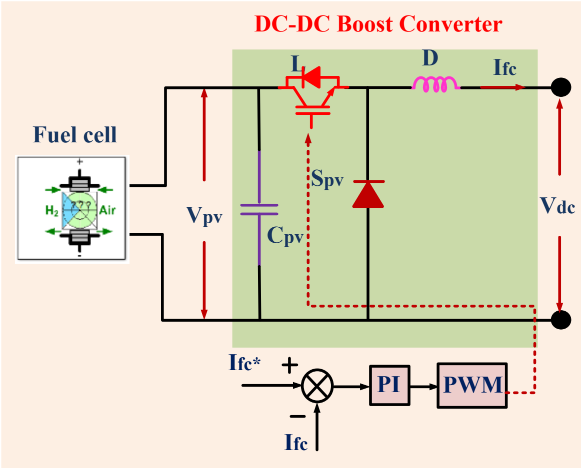

Fig. 4. Fuel cell system with PI-controlled DC–DC boost converter.

B. Fuel Cell Mathematical Model

The output voltage of a proton exchange membrane fuel cell (PEMFC) is expressed as

$$V_{FC} = E_N - V_{act} - V_{ohm} - V_{con} \quad (19)$$

where

- E_N = Nernst voltage (V)
- V_{act} = activation loss (V)
- V_{ohm} = ohmic loss (V)
- V_{con} = concentration loss (V)

The Nernst voltage is

$$E_N = E_0 + \frac{RT}{2F} In\left(\frac{P_{H_2}\sqrt{P_{O_2}}}{P_{H_2}O}\right) \quad (20)$$

where

- R=8.314 J/mol\cdotpK
- T = operating temperature (K)
- F=96485 C/mol
- $P_{H_2}, P_{O_2}, P_{H_2}O$ are the partial pressures.

The activation voltage loss is

$$V_{aCt} = A\, In\left(\frac{I_{Fc}}{I_o}\right) \quad (21)$$

where

- A = Tafel slope
- I_o = exchange current.

The ohmic loss is

$$V_{ohm} = I_{FC} R_{int} \quad (22)$$

where

R_{int} is the internal resistance of the fuel cell.

The concentration loss is

$$V_{con} = -B\, In\left(1 - \frac{I_{Fc}}{I_{lim}}\right) \quad (23)$$

where

- B = concentration coefficient
- I_{lim} = limiting current.

The output power supplied by the fuel cell

$$P_{FC} = V_{FC} I_{Fc} \quad (24)$$

D. PI Current Controller

The fuel cell current is regulated using a PI controller.

The current error is

$$e(t) = I_{FC}^{*} - I_{Fc} \quad (25)$$

The controller output is

$$u(t) = K_p e(t) + K_i \int e(t)\, dt \quad (26)$$

where

- K_p = proportional gain
- K_i = integral gain.

The PWM duty cycle is generated as

$$D = \frac{u(t)}{V_C} \quad (27)$$

where V_C is the carrier signal amplitude.

The generated PWM pulses control the switching device of the boost converter, ensuring that the fuel cell current follows its reference value while maintaining a regulated DC bus voltage and stable power transfer.

V. Battery Energy Storage System Modeling and Bidirectional DC–DC Buck–Boost Converter

A. System Configuration

The Battery Energy Storage System (BESS) provides energy balancing and DC bus voltage support in the proposed hybrid DC microgrid. As shown in Fig. 5, the battery is connected to the common 600 V DC bus through a bidirectional DC–DC buck–boost converter consisting of an inductor Lb, capacitor Cb, and two complementary switches Sb1 and Sb2. The converter enables bidirectional power flow, allowing the battery to operate in both charging and discharging modes. During surplus renewable energy generation, the converter operates in buck mode to charge the battery, whereas during renewable power deficiency it operates in boost mode to discharge the battery and maintain the DC bus voltage.

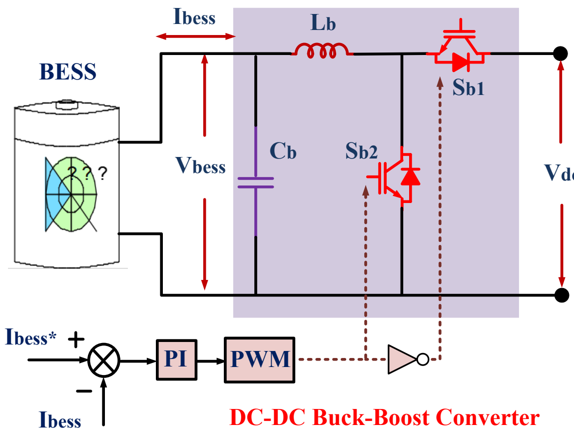

Fig. 5. Battery energy storage system with bidirectional DC–DC buck–boost converter.

B. Battery Mathematical Model

The battery terminal voltage is expressed as

$$V_{BESS} = E_{oc} - I_{BESS} R_{int} \quad (28)$$

where

- E_{oc} = open-circuit voltage (V)
- I_{BESS} = battery current (A)
- R_{int} = internal resistance (Ω).

The battery output power is

$$P_{BESS} = V_{BESS} I_{BESS} \quad (29)$$

The Battery State of Charge (SOC) is calculated as

$$SOC(t) = SOC_0 - \frac{1}{Q_{bat}} \int_0^t I_{BESS}(t)\, dt \quad (30)$$

where

- SOC_0 = initial state of charge
- Q_{bat} = battery capacity (Ah).

For charging,

$I_{BESS} < 0$

For discharging,

$I_{BESS} > 0$

D. Battery Current Controller

The bidirectional converter regulates the battery current using a PI controller.

The current error is

$$e(t) = I^*_{BESS} - I_{BESS} \quad (31)$$

The PI controller output is

$$u(t) = K_P e(t) + K_i \int e(t)\, dt \quad (32)$$

The PWM duty cycle is

$$D = \frac{u(t)}{V_C} \quad (33)$$

Where

- K_p = proportional gain
- K_i = integral gain
- V_c = carrier signal amplitude.

The generated PWM pulses control switches Sb1 and Sb2 , enabling smooth transition between charging and discharging modes while maintaining a stable DC bus voltage and efficient energy management.

VI. Supercapacitor Modeling and Bidirectional DC–DC Buck–Boost Converter

A. System Configuration

The supercapacitor (SC) is incorporated into the proposed hybrid DC microgrid to compensate for rapid power fluctuations and improve the transient response of the system. As shown in Fig. 6, the supercapacitor is interfaced with the common 600 V DC bus through a bidirectional DC–DC buck–boost converter consisting of an inductor Lsc, capacitor Csc, and two complementary switches Ssc1 and Ssc2. The converter enables bidirectional power flow, allowing the supercapacitor to absorb excess energy during charging and supply high transient power during discharging. Consequently, the supercapacitor minimizes battery current stress and enhances the dynamic stability of the DC microgrid.

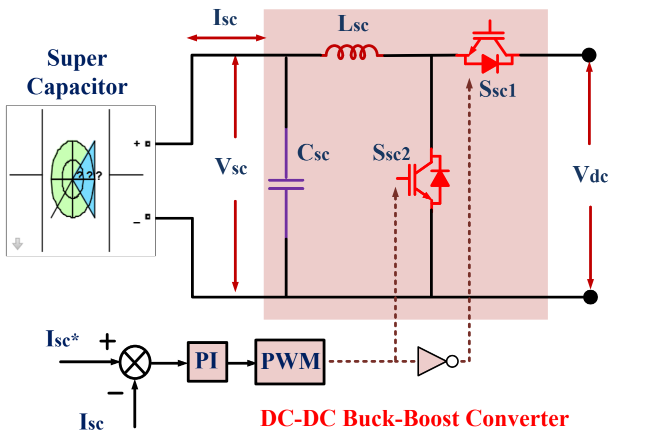

Fig. 6. Supercapacitor with bidirectional DC–DC buck–boost converter.

B. Supercapacitor Mathematical Model

The supercapacitor terminal voltage is expressed as

$$v_{sc} = V_{SCO} + \frac{1}{C_{sc}} \int I_{sc}\, dt \quad (34)$$

where

- V_{SCO} = initial supercapacitor voltage (V)
- C_{sc} = supercapacitor capacitance (F)
- I_{sc} = supercapacitor current (A).

The stored energy in the supercapacitor is

$$E_{sc} = \frac{1}{2} C_{sc} V_{sc}^2 \quad (35)$$

The output power is

$$P_{sc} = V_{sc} I_{sc} \quad (36)$$

D. Supercapacitor Current Controller

The supercapacitor current is controlled using a PI controller.

The current error is

$$e(t) = I^*_{sc} - I_{sc} \quad (37)$$

The PI controller output is

$$u(t) = K_P e(t) + K_i \int e(t)\, dt \quad (38)$$

The PWM duty cycle is generated as

$$D = \frac{u(t)}{V_C} \quad (39)$$

The PWM signals control the switches Ssc1 and Ssc2, enabling seamless transition between charging and discharging modes. The supercapacitor rapidly compensates transient power variations, thereby maintaining DC bus voltage stability and reducing the charging/discharging stress on the battery energy storage system.

VII. Three-Phase Voltage Source Converter

A. System Configuration

The three-phase Voltage Source Converter (VSC) provides the interface between the hybrid DC microgrid and the utility grid, as shown in Fig. 7. The converter consists of six insulated gate bipolar transistor (IGBT) switches (S1–S6), a DC-link capacitor Cdc, and an LCL filter comprising converter-side inductance (Lf), grid-side inductance (Lg), and filter capacitor (Cf). The VSC enables bidirectional power flow between the DC microgrid and the utility grid while maintaining the DC bus voltage at 600 V. A Phase-Locked Loop (PLL) synchronizes the converter with the grid voltage, whereas a hysteresis current controller generates the switching pulses based on the reference and measured grid currents. The converter performs DC bus voltage regulation, active power transfer, reactive power compensation, harmonic mitigation, and grid synchronization.

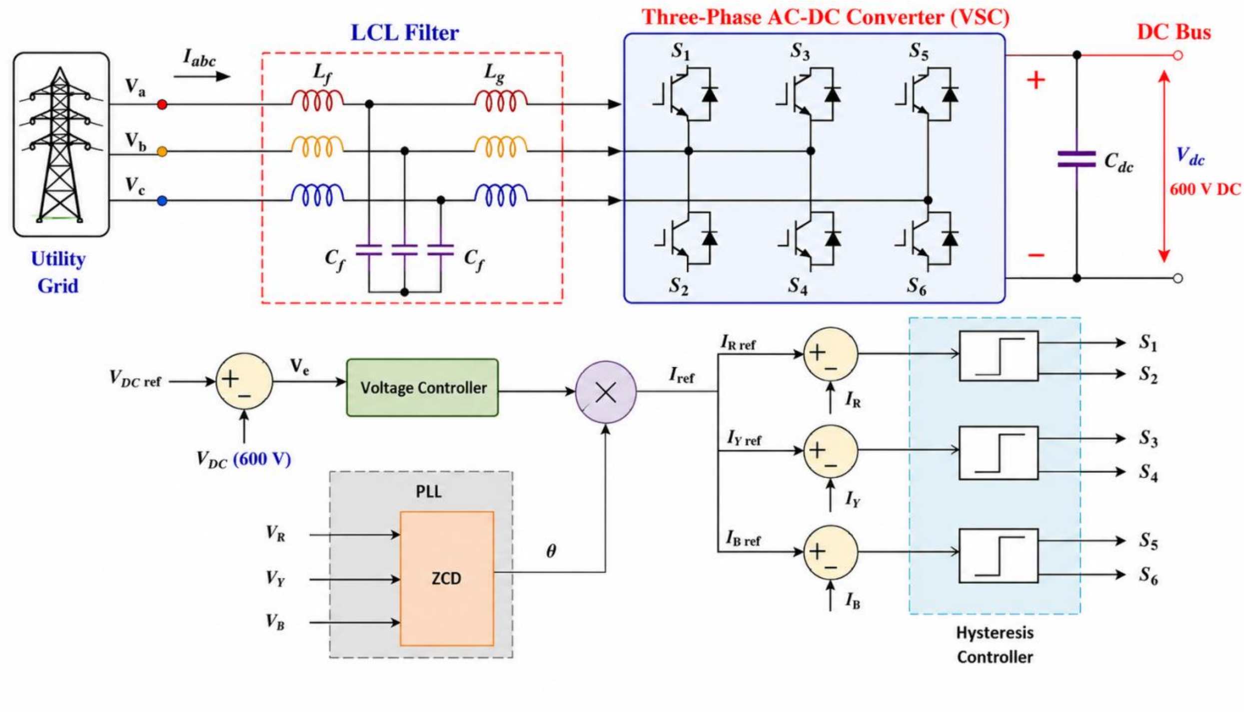

Fig. 7. Three-phase voltage source converter and hysteresis current controller.

B. Voltage Source Converter Modeling

The three-phase converter output voltage is expressed as

$$V_{abc} = S_{abc} V_{dc} \quad (40)$$

where

- V_{dc} = DC bus voltage
- S_{abc} = switching function vector.

The active power exchanged between the converter and the grid is

$$P = \frac{3}{2}(V_d i_d + V_q i_q) \quad (42)$$

The reactive power is

$$Q = \frac{3}{2}(V_q i_d - V_d i_q) \quad (43)$$

The DC-link capacitor dynamics are

$$C_{dc}\frac{dV_{dc}}{dt} = I_{dc} - I_{VSC} \quad (44)$$

where

- I_{dc} = DC source current
- I_{VSC} = converter current.

C. LCL Filter Design

The converter-side inductance is selected as

$$L_f = \frac{V_{dc}}{6 f_s \Delta I} \quad (45)$$

The filter capacitor is

$$C_f = \frac{0.05P}{2\pi f V_g^2} \quad (46)$$

The grid-side inductance is

$$L_g = (0.2 \sim 0 \cdot 3)L_f \quad (47)$$

The resonance frequency of the LCL filter is

$$f_r = \frac{1}{2\pi}\sqrt{\frac{L_f + L_g}{L_f L_g C_f}} \quad (48)$$

where

- fs = switching frequency
- P = rated converter power
- Vg = grid voltage.

D. DC Bus Voltage Controller

The DC bus voltage error is calculated as

$$e_v = V_{dc}^* - V_{dc} \quad (49)$$

The PI controller generates the reference current

$$I_{ref} = k_P e_v + K_i \int e_v \, dt \quad (50)$$

where

- k_P = proportional gain
- K_i = integral gain.

E. Phase-Locked Loop (PLL)

The PLL estimates the grid phase angle for synchronization.

The phase angle is

$$\theta = tan^{-1}\left(\frac{V_\beta}{V_\alpha}\right) \quad (51)$$

where

- V_α and V_β are the stationary reference frame voltages.

F. Hysteresis Current Controller

The reference current is compared with the measured grid current.

The current error is

$$e_i = I_{ref} - I_g \quad (52)$$

The switching logic is

$$\begin{cases} S = 1, e_i > H \\ S = 0, e_i < -H \end{cases} \quad (53)$$

where

- H = hysteresis band.

The generated switching pulses control switches S1-S6, ensuring accurate current tracking and fast dynamic response.

VIII. Simulation Results and Discussion

A. Solar PV System Performance

The performance of the proposed photovoltaic (PV) system is evaluated under varying solar irradiance conditions to verify the effectiveness of the P&O MPPT algorithm and the DC–DC boost converter, as shown in Fig. 8. The solar irradiance is gradually reduced from 1000 W/m² to 750 W/m², 500 W/m², and finally 300 W/m² at different time intervals to emulate realistic weather variations.

As illustrated in Fig. 8(b), the PV output voltage remains nearly constant at approximately 300 V, despite the changes in irradiance, demonstrating the effective regulation capability of the boost converter and the MPPT controller. The PV output current shown in Fig. 8(c) decreases proportionally with the reduction in irradiance, varying from approximately 145 A to 45 A. Similarly, the PV output power in Fig. 8(d) decreases from approximately 42 kW under standard irradiance to about 13 kW at 300 W/m², following the available solar energy. The response is smooth with minimal transient oscillations, indicating fast dynamic tracking and stable converter operation. These results confirm that the proposed PV system efficiently extracts the maximum available power under varying environmental conditions while maintaining stable operation of the common DC bus.

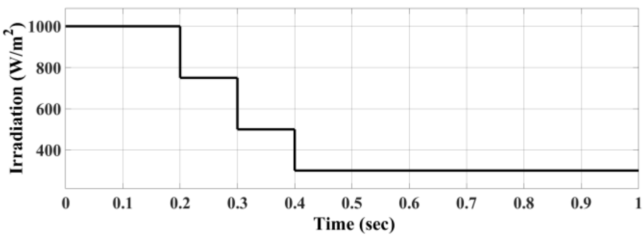

(a)

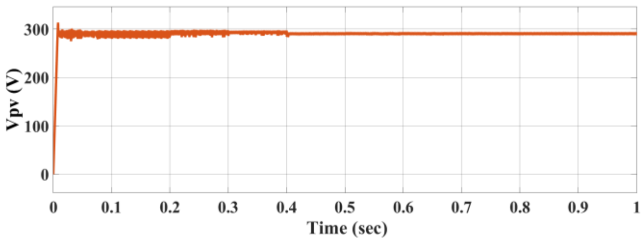

(b)

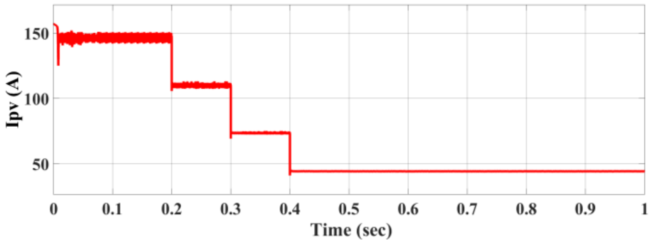

(c)

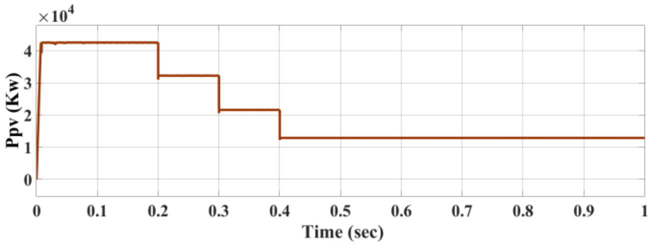

(d)

Fig. 8. Performance of the PV system under varying irradiance conditions: (a) solar irradiance, (b) PV output voltage, (c) PV output current, and (d) PV output power.

B. Battery and Supercapacitor Performance

The dynamic performance of the Battery Energy Storage System (BESS) and the supercapacitor (SC) is evaluated under varying operating conditions, as shown in Fig. 9. Fig. 9(a) illustrates the battery terminal voltage, which remains nearly constant at approximately 324 V throughout the simulation, indicating effective voltage regulation by the bidirectional DC–DC buck–boost converter. The battery current shown in Fig. 9(b) varies according to the power demand, where negative current represents charging and positive current indicates discharging operation. Correspondingly, the battery power in Fig. 9(c) changes smoothly between charging and discharging modes, ensuring balanced energy exchange with the DC bus. The battery State of Charge (SOC) presented in Fig. 9(d) remains nearly constant around 63.81%, with only a slight increase during the simulation, confirming reduced battery stress and controlled charging/discharging cycles.

The supercapacitor performance is depicted in Fig. 9(e) and Fig. 9(f). The supercapacitor current rapidly responds to transient load variations, while the corresponding power exhibits fast bidirectional compensation during sudden changes in system demand. Owing to its high power density and fast dynamic response, the supercapacitor effectively absorbs and delivers transient power, thereby reducing battery current fluctuations and improving the stability of the common DC bus. These results demonstrate the coordinated operation of the battery and supercapacitor, ensuring efficient energy management, enhanced dynamic response, and improved reliability of the proposed hybrid DC microgrid.

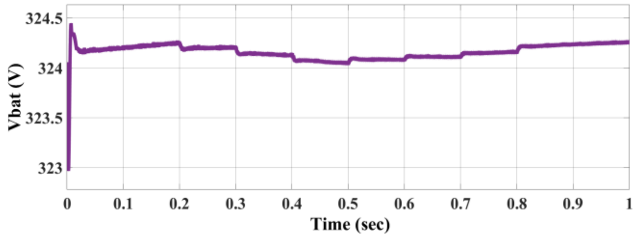

(a)

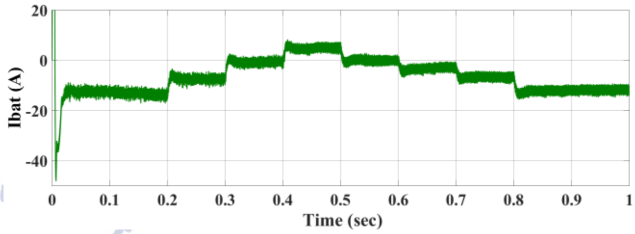

(b)

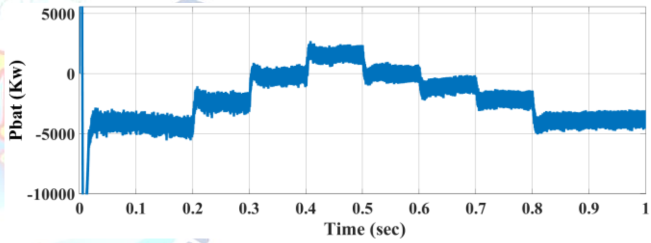

(c)

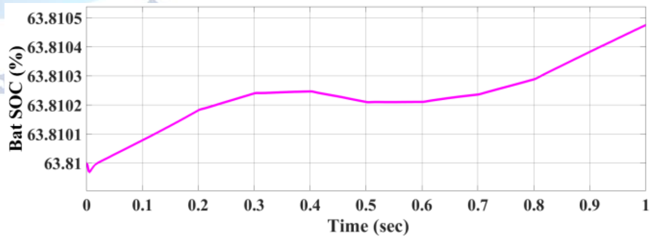

(d)

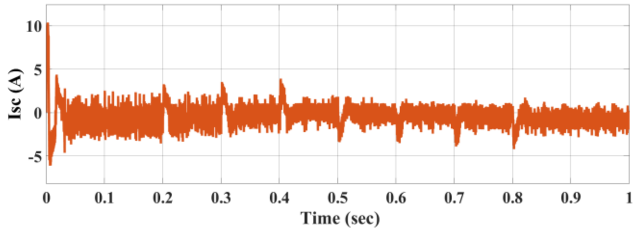

(e)

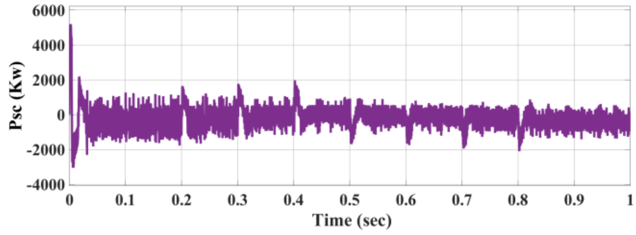

(f)

Fig. 9. Performance of the hybrid energy storage system: (a) battery voltage, (b) battery current, (c) battery power, (d) battery state of charge, (e) supercapacitor current, and (f) supercapacitor power.

C. Fuel Cell Performance

The performance of the fuel cell (FC) is evaluated under varying load demand to verify its dynamic response and power support capability, as shown in Fig. 10. Fig. 10(a) illustrates the reference fuel cell current, which is increased in a stepwise manner from 0 A to 50 A between 0.5 s and 0.8 s to emulate increasing power demand. As shown in Fig. 10(b), the actual fuel cell current accurately tracks the reference current with a fast transient response and negligible steady-state error, demonstrating the effectiveness of the PI-controlled DC–DC boost converter.

The corresponding fuel cell output power is presented in Fig. 10(c). The output power increases proportionally with the reference current, reaching approximately 30 kW at the maximum operating condition. The smooth transition between operating levels and the absence of significant oscillations indicate stable converter operation and efficient power regulation. These results confirm that the fuel cell effectively provides supplementary power during increased load demand, thereby enhancing the reliability, power-sharing capability, and stability of the proposed hybrid DC microgrid.

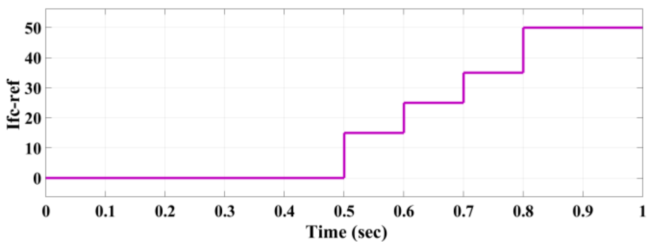

(a)

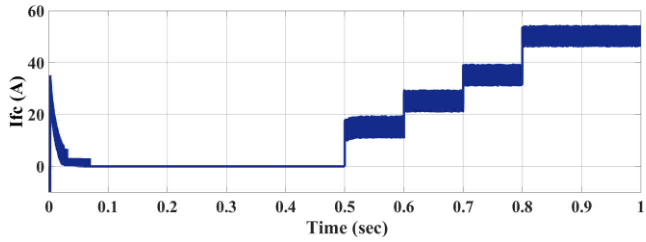

(b)

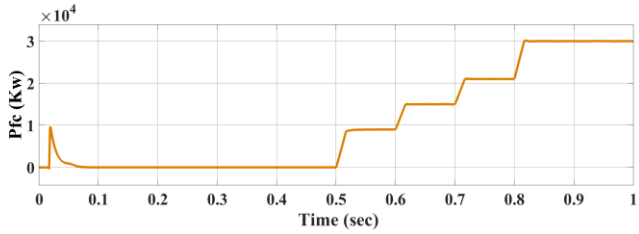

(c)

Fig. 10. Fuel cell performance: (a) reference fuel cell current, (b) fuel cell current, and (c) fuel cell output power.

D. Grid-Connected Microgrid Performance

The grid-connected performance of the proposed hybrid DC microgrid is evaluated under varying operating conditions, as shown in Fig. 11. Fig. 11(a) illustrates the three-phase grid voltage, which remains balanced and sinusoidal throughout the simulation with a peak amplitude of approximately ±325 V (230 V RMS per phase), confirming effective synchronization with the utility grid. The corresponding three-phase grid current shown in Fig. 11(b) varies according to the power exchanged between the microgrid and the utility grid. Initially, the grid current reaches approximately ±70 A and subsequently varies between ±5 A and ±40 A depending on renewable power generation and load demand, demonstrating stable bidirectional power flow.

The nonlinear load current presented in Fig. 11(c) exhibits a peak amplitude of approximately ±22 A, while the linear load current in Fig. 11(d) remains sinusoidal with a peak value of approximately ±15 A, confirming the capability of the proposed system to supply both nonlinear and linear loads simultaneously. The grid active power shown in Fig. 11(e) varies smoothly between approximately −30 kW (grid import) and +10 kW (grid export), indicating efficient bidirectional power exchange according to the operating conditions.

The DC bus voltage response is illustrated in Fig. 11(f). After a short startup transient of approximately 700 V, the DC bus voltage quickly settles and is regulated around the reference value of 600 V, with only minor voltage deviations of approximately ±5 V during load and power transitions. These results demonstrate that the proposed VSC control strategy effectively maintains DC bus voltage regulation, ensures stable grid synchronization, supports bidirectional power transfer, and enhances the overall power quality of the hybrid DC microgrid.

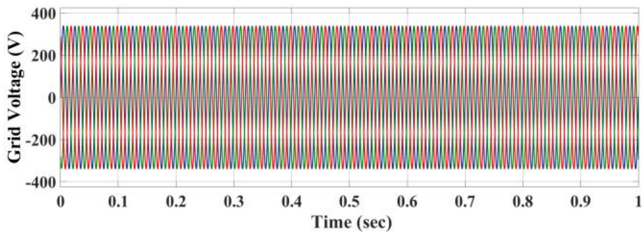

(a)

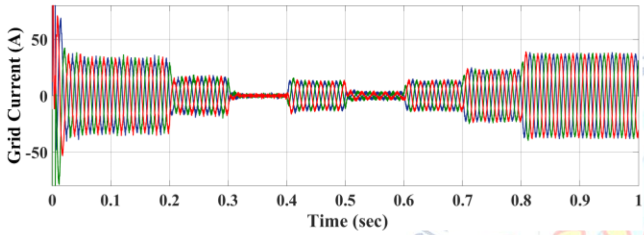

(b)

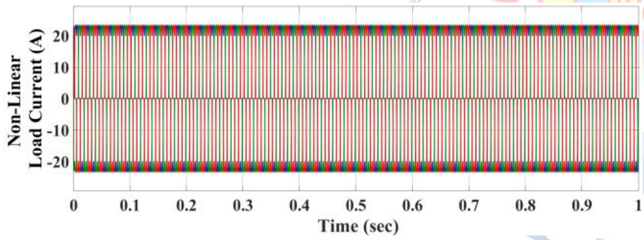

(c)

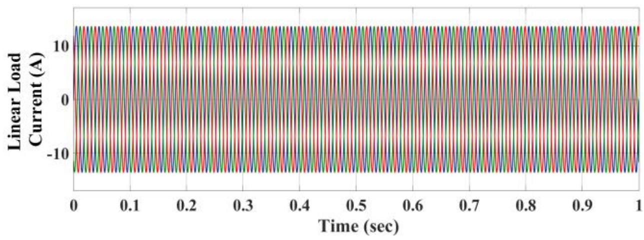

(d)

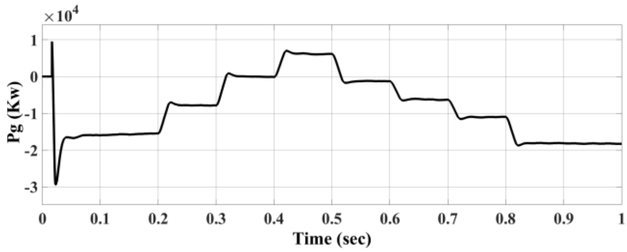

(e)

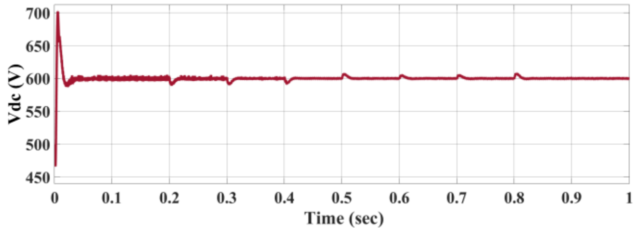

(f)

Fig. 11. Grid-connected microgrid performance: (a) grid voltage, (b) grid current, (c) nonlinear load current, (d) linear load current, (e) grid active power, and (f) DC bus voltage.

IX. Conclusion

This paper presented an intelligent energy management strategy for a grid-connected hybrid DC microgrid integrating a solar photovoltaic (PV) array, fuel cell (FC), battery energy storage system (BESS), and supercapacitor (SC). The proposed system effectively coordinated power sharing among the renewable sources and energy storage devices while maintaining a stable 600 V DC bus under varying operating conditions. Simulation results verified efficient maximum power extraction from the PV system, reliable fuel cell power support, effective battery–supercapacitor coordination, and stable bidirectional power exchange with the utility grid. Moreover, the proposed VSC control strategy ensured improved DC bus voltage regulation, grid synchronization, and power quality while supplying both linear and nonlinear loads. Overall, the proposed hybrid DC microgrid demonstrated enhanced renewable energy utilization, system stability, and reliable operation, making it a suitable solution for future smart grid applications.

Conflict of interest statement

Authors declare that they do not have any conflict of interest.

References

[1] R. Geetha, S. Gunanandhini, G. Umarani Srikanth, and V. Sujatha, "Human Stress Detection in and Through Sleep Patterns Using Machine Learning Algorithms," Journal of The Institution of Engineers (India): Series B, vol. 105, no. 6, pp. 1691–1713, 2024. doi: 10.1007/s40031-024-01079-y.

[2] [1] M. A. Koondhar, I. A. Laghari, B. M. Asfaw, R. Reji Kumar, and A. H. Lenin, ''Experimental and simulation-based comparative analysis of different parameters of PV module,'' Sci. Afr., vol. 16, Jul. 2022, Art. no. e01197.

[3] [2] J. Zheng, J. Du, B. Wang, J. J. Klemeš, Q. Liao, and Y. Liang, ''A hybrid framework for forecasting power generation of multiple renewable energy sources,'' Renew. Sustain. Energy Rev., vol. 172, Feb. 2023, Art. no. 113046.

[4] [3] A. M. Shaheen, A. M. Elsayed, A. R. Ginidi, E. E. Elattar, and R. A. El-Sehiemy, ''Effective automation of distribution systems with joint integration of DGs/SVCs considering reconfiguration capability by jellyfish search algorithm,'' IEEE Access, vol. 9, pp. 92053–92069, 2021.

[5] [4] M. A. Koondhar, I. A. Channa, S. Chandio, M. I. Jamali, A. S. Channa, and I. A. Laghari, ''Temperature and irradiance based analysis the specific variation of PV module,'' Jurnal Teknologi, vol. 83, no. 6, pp. 1–17, Sep. 2021.

[6] [5] E. M. Vicente, P. Santos Vicente, R. L. Moreno, and E. R. Ribeiro, ''High-efficiency MPPT method based on irradiance and temperature measurements,'' IET Renew. Power Gener., vol. 14, no. 6, pp. 986–995, Apr. 2020.

[7] [6] N. Das, H. Wongsodihardjo, and S. Islam, ''Modeling of multi-junction photovoltaic cell using MATLAB/SIMULINK to improve the conversion efficiency,'' Renew. Energy, vol. 74, pp. 917–924, Feb. 2015.

[8] [7] A. Abu-Siada and S. M. Islam, ''Applications of power electronics in renewable energy systems,'' in Power Electronics Handbook. Amsterdam, The Netherlands: Elsevier, 2024, pp. 797–843.

[9] [8] V. S. Nayagam, A. P. Jyothi, P. Abirami, J. Femila Roseline, M. Sudhakar, E. A. Al-Ammar, S. M.Wabaidur, N. Hoda, and A. Sisay, ''Deep learning model on energy management in grid-connected solar systems,'' Int. J. Photoenergy, vol. 2022, pp. 1–8, May 2022.

[10] [9] J. D. Vergara-Dietrich, M. M. Morato, P. R. C. Mendes, A. A. Cani, J. E. Normey-Rico, and C. Bordons, ''Advanced chance-constrained predictive control for the efficient energy management of renewable power systems,'' J. Process Control, vol. 74, pp. 120–132, Feb. 2019.

[11] [10] D. Azuatalam, K. Paridari, Y. Ma, M. Förstl, A. C. Chapman, and G. Verbič, ''Energy management of small-scale PV-battery systems: Asystematic reviewconsidering practical implementation, computational requirements, quality of input data and battery degradation,'' Renew. Sustain. Energy Rev., vol. 112, pp. 555–570, Sep. 2019.

[12] [11] M. Alhussein, S. I. Haider, and K. Aurangzeb, ''Microgrid-level energy management approach based on short-term forecasting of wind speed and solar irradiance,'' Energies, vol. 12, no. 8, p. 1487, Apr. 2019.

[13] [12] B. Benlahbib, N. Bouarroudj, S. Mekhilef, D. Abdeldjalil, T. Abdelkrim, F. Bouchafaa, and A. Lakhdari, ''Experimental investigation of power management and control of a PV/wind/fuel cell/battery hybrid energy system microgrid,'' Int. J. Hydrogen Energy, vol. 45, no. 53, pp. 29110–29122, Oct. 2020.

[14] [13] A. Colmenar-Santos, M. Monteagudo-Mencucci, E. Rosales-Asensio, M. de Simón-Martín, and C. Pérez-Molina, ''Optimized design method for storage systems in photovoltaic plants with delivery limitation,'' Sol. Energy, vol. 180, pp. 468–488, Mar. 2019.

[15] [14] R. Siddaiah and R. P. Saini, ''A review on planning, configurations, modeling and optimization techniques of hybrid renewable energy systems for off grid applications,'' Renew. Sustain. Energy Rev., vol. 58, pp. 376–396, May 2016.

[16] [15] T. Ma and M. S. Javed, ''Integrated sizing of hybrid PV-wind-battery system for remote island considering the saturation of each renewable energy resource,'' Energy Convers. Manage., vol. 182, pp. 178–190, Feb. 2019.

[17] [16] O. Majeed Butt, M. Zulqarnain, and T. Majeed Butt, ''Recent advancement in smart grid technology: Future prospects in the electrical power network,'' Ain Shams Eng. J., vol. 12, no. 1, pp. 687–695, Mar. 2021.

[18] [17] Y. Zhang, Y. Yang, and L. Dai, ''Energy efficiency maximization for device-to-device communication underlaying cellular networks on multiple bands,'' IEEE Access, vol. 4, pp. 7682–7691, 2016.

[19] [18] M. Dashtdar, M. Bajaj, and S. M. S. Hosseinimoghadam, ''Design of optimal energy management system in a residential microgrid based on smart control,'' Smart Sci., vol. 10, no. 1, pp. 25–39, Jan. 2022.

[20] [19] J. Jurasz, F. A. Canales, A. Kies, M. Guezgouz, and A. Beluco, ''Areviewon the complementarity of renewable energy sources: Concept, metrics, application and future research directions,'' Sol. Energy, vol. 195, pp. 703–724, Jan. 2020.

[21] [20] S. Alatai, M. Salem, D. Ishak, H. S. Das, M. A. Nazari, A. Bughneda, and M. Kamarol, ''A review on state-of-the-art power converters: Bidirectional, resonant, multilevel converters and their derivatives,'' Appl. Sci., vol. 11, no. 21, p. 10172, Oct. 2021.

[22] [21] S. Saravanan and N. Ramesh Babu, ''Analysis and implementation of high step-up DC–DC converter for PV based grid application,'' Appl. Energy, vol. 190, pp. 64–72, Mar. 2017.

[23] [22] E. Kabalci, Multilevel Inverters: Control Methods and Advanced Power Electronic Applications. New York, NY, USA: Academic, 2021.

[24] [23] F. Mumtaz, N. Zaihar Yahaya, S. Tanzim Meraj, B. Singh, R. Kannan, and O. Ibrahim, ''Review on non-isolated DC–DC converters and their control techniques for renewable energy applications,'' Ain Shams Eng. J., vol. 12, no. 4, pp. 3747–3763, Dec. 2021.

[25] [24] A. Kolli, A. Gaillard, A. De Bernardinis, O. Bethoux, D. Hissel, and Z. Khatir, ''A review on DC/DC converter architectures for power fuel cell applications,'' Energy Convers. Manage., vol. 105, pp. 716–730, Nov. 2015.

[26] [25] M. J. Khan and L. Mathew, ''Comparative study of maximum power point tracking techniques for hybrid renewable energy system,'' Int. J. Electron., vol. 106, no. 8, pp. 1216–1228, Aug. 2019.

[27] [26] T. Arunkumari and V. Indragandhi, ''An overview of high voltage conversion ratio DC–DC converter configurations used in DC micro-grid architectures,'' in Proc. Renew. Sustain. Energy Rev., vol. 77, Apr. 2017, pp. 670–687.

[28] [27] P. E. Bett and H. E. Thornton, ''The climatological relationships between wind and solar energy supply in Britain,'' Renew. Energy, vol. 87, pp. 96–110, Mar. 2016.

[29] [28] S. Sharma, Y. R. Sood, N. K. Sharma, M. Bajaj, H. M. Zawbaa, R. A. Turky, and S. Kamel, ''Modeling and sensitivity analysis of gridconnected hybrid green microgrid system,'' Ain Shams Eng. J., vol. 13, no. 4, Jun. 2022, Art. no. 101679.